

Improved Decoding of Quantum Tanner Codes Using Generalized Check Nodes

Olai Å. Mostad, *Student Member, IEEE*, Eirik Rosnes, *Senior Member, IEEE*, and Hsuan-Yin Lin, *Senior Member, IEEE*

Abstract—We study the decoding problem for quantum Tanner codes and propose to exploit the underlying local code structure by grouping check nodes into more powerful generalized check nodes for enhanced iterative belief propagation (BP) decoding by decoding the generalized checks using a maximum a posteriori (MAP) decoder as part of the check node processing of each decoding iteration. We mainly study the finite-length setting and show that the proposed enhanced generalized BP decoder for quantum Tanner codes significantly outperforms the standard quaternary BP decoder with memory effects, as well as the recently proposed Relay-BP decoder, even outperforming generalized bicycle (GB) codes with comparable parameters in some cases. For other classes of quantum low-density parity-check (qLDPC) codes, we propose a greedy algorithm to combine checks for generalized BP decoding. However, for GB codes, bivariate bicycle codes, hypergraph product codes, and lifted-product codes, there seems to be limited gain by combining simple checks into more powerful ones. To back up our findings, we also provide a theoretical cycle analysis for the considered qLDPC codes.

I. INTRODUCTION

Efficient and improved decoding of quantum low-density parity-check (qLDPC) codes has recently received significant attention, see, e.g., [1]–[7] and references therein, as iterative belief propagation (BP) decoding (both binary and nonbinary) in general performs worse than for classical LDPC codes. The degraded performance can usually be explained by a larger number of 4-cycles in the underlying Tanner graphs and a large number of degenerate errors, i.e., correctable errors affecting the logical state equally as different correctable errors.

In this work, we propose to exploit the underlying local code structure of quantum Tanner codes [8] for improved iterative BP decoding, in the sense of exploiting a natural grouping of check nodes into *generalized* checks that can be decoded using a maximum a posteriori (MAP) decoder as part of the check node processing of each decoding iteration. The quantum Tanner codes are constructed from a certain type of square complex by placing bits on the squares and constraints on the vertices. These constraints are more involved than single parity-checks, but can still be viewed as single generalized checks for iterative BP decoding. We also consider the intermediate case, where some checks per vertex are combined but not all. The idea here is similar to classical generalized LDPC codes first introduced by Tanner [9] and later extensively investigated (see, e.g., [10] and references

therein). The proposed solution can be added to any iterative BP decoder for qLDPC codes, by combining checks of the parity-check matrix (preferably with meaningful overlap) into generalized checks. However, we have only observed limited gains for other classes of qLDPC codes, like generalized bicycle (GB) codes [11], [12], bivariate bicycle (BB) codes [13], hypergraph product (HGP) codes [14], [15], and lifted-product (LP) codes [16]. Here, we combine the method with quaternary (BP₄) decoding with additional memory effects [3, Alg. 1], denoted by MBP₄, combined with ordered statistics decoding (OSD) for post-processing [12]. Our focus is on short-to-medium length quantum Tanner codes, i.e., the so-called finite-length regime. So far, there is limited work on this regime for quantum Tanner codes, except for a few recent works [17]–[20]. We show by simulation that the proposed decoder can significantly outperform conventional MBP₄+OSD-1 and the recently proposed Relay-BP (“Relay-ensembling with locally-averaged memory”) decoder [4, Alg. 1] for small-to-medium length quantum Tanner codes.

As the number of 4-cycles in the Tanner graph is important for the performance of a BP decoder, we give a description of the 4-cycles of the Tanner graphs of quantum Tanner codes, both for the usual BP decoders and the proposed one. From this description, we derive a criterion that guarantees no 4-cycles for a binary decoder and show how to calculate the number of 4-cycles for a quaternary decoder. We also provide a similar description for HGP codes, and argue that the descriptions for quantum Tanner codes and HGP codes together give such a description for LP codes.

Our main contributions can be summarized as follows.

- 1) Our proposed generalized MBP₄ decoder significantly outperforms the conventional MBP₄ decoder for quantum Tanner codes with and without OSD post-processing of order 1 on the depolarization channel, at the expense of a higher decoding complexity. Interestingly, contrary to the case of the conventional MBP₄ decoder, OSD post-processing is not necessary in order to approach the best performance with the generalized MBP₄ decoder. However, when applied to other classes of qLDPC codes, like GB, BB, LP, and HGP codes, our simulations show no noticeable performance gain by combining simple checks into more powerful generalized checks.
- 2) Building upon the previous point, we show examples where quantum Tanner codes outperform optimized GB codes, LP codes, and HGP codes with comparable parity-check row weights when decoded with the proposed generalized decoder. Moreover, as illustrated in Fig. 3, for a

Olai Å. Mostad, E. Rosnes, and H.-Y. Lin are with Simula UiB, N-5006 Bergen, Norway (e-mail: olai@simula.no, eirikrosnes@simula.no, lin@simula.no).

[[432, 16, ≤ 26]] quantum Tanner code from [20, Tab. 2], when combining only three checks into each generalized check, our proposed decoder shows a significantly performance improvement compared to Relay-BP₄, even with what seems to be a lower overall decoding complexity. This example shows that the proposed decoder can also possess a favorable performance-complexity trade-off.

- 3) Finally, our findings summarized above have been backed up theoretically by providing a cycle analysis for the considered qLDPC codes.

A. Notation

Vectors are denoted by bold letters, matrices by sans serif uppercase letters, and sets (and groups) by calligraphic uppercase letters, e.g., \mathbf{a} , \mathbf{A} , and \mathcal{A} , respectively. The neutral element of a group will be denoted by 1, while e is reserved for an edge in a graph. Linear codes, graphs, and square complexes are denoted by script uppercase letters, e.g., \mathcal{C} . A graph with vertex set \mathcal{V} and edge set \mathcal{E} is denoted by $\mathcal{G} = (\mathcal{V}, \mathcal{E})$, and may have parallel edges and self-loops unless stated otherwise. The edges incident to a vertex v is called the local view of v and denoted $\mathcal{E}(v)$. We work with undirected graphs with an ordering on the edges. The disjoint union of sets \mathcal{A}, \mathcal{B} is denoted by $\mathcal{A} \sqcup \mathcal{B} \triangleq \{(a, 0), (b, 1) : a \in \mathcal{A}, b \in \mathcal{B}\}$. A linear code \mathcal{C} of length n , dimension k , and minimum distance d is sometimes referred to by $[n, k, d]$, and its dual code is denoted \mathcal{C}^\perp . The binary field is denoted by \mathbb{F}_2 , while \mathbb{C} denotes the complex numbers. Standard order notation $\Theta(\cdot)$ and $O(\cdot)$ is used for asymptotic results. Given natural numbers a and b , we let $[a] \triangleq \{1, 2, \dots, a\}$, $[a : b] \triangleq \{a, a + 1, \dots, b\}$, for $a \leq b$, and $[a : b] \triangleq \{a, a - 1, \dots, b\}$ for $a > b$. For real numbers a and b , we define $\max^*(a, b) \triangleq \max(a, b) + \log(1 + e^{-|a-b|})$ and denote the component-wise logical OR of $\mathbf{a}, \mathbf{b} \in \mathbb{F}_2^n$ by $\mathbf{a} \vee \mathbf{b}$, that is, $(\mathbf{a} \vee \mathbf{b})_i \triangleq a_i \vee b_i$. A quantum code with length n and code dimension k is denoted as $[[n, k]]$, or more explicitly as $[[n, k, d]]$ when the minimum distance d is specified. For the four Pauli matrices, we use the notation

$$I \triangleq \begin{bmatrix} 1 & 0 \\ 0 & 1 \end{bmatrix}, \quad X \triangleq \begin{bmatrix} 0 & 1 \\ 1 & 0 \end{bmatrix}, \quad Y \triangleq \begin{bmatrix} 0 & -i \\ i & 0 \end{bmatrix}, \quad Z \triangleq \begin{bmatrix} 1 & 0 \\ 0 & -1 \end{bmatrix}.$$

Given n Pauli matrices $W_i \in \{I, X, Y, Z\}$, the Kronecker product $\bigotimes_{i=1}^n W_i$ is called a Pauli string, denoted by \mathbf{W} , and often considered as row vectors $[W_1, \dots, W_n]$. The operator \boxplus (referred to as box-plus) is defined by

$$\boxplus_{i=1}^{\kappa} a_i \triangleq 2 \tanh^{-1} \left(\prod_{i=1}^{\kappa} \tanh \frac{a_i}{2} \right),$$

for $a_1, \dots, a_\kappa \in \mathbb{R}$. Finally, we define \bar{i} as the complement of $i \in \{0, 1\}$, i.e., $\bar{i} = 1$ for $i = 0$ and 0 for $i = 1$, and let $W_0 = X$ and $W_1 = Z$.

II. PRELIMINARIES

We recall background on graphs related to error correction, the notion of quantum error-correcting codes, some particular constructions of quantum error-correcting codes, and the channel we consider for decoding. At the reader's discretion, this section can safely be skipped and referred back to later when needed.

A. Graph Constructions

Definition 1 (Incidence graph). *The (vertex-edge) incidence graph of a graph $\mathcal{G} = (\mathcal{V}, \mathcal{E})$ is the bipartite graph $I(\mathcal{G})$ with vertices $\mathcal{V} \sqcup \mathcal{E}$ and an edge (v, e) for every $e \in \mathcal{E}$ incident to $v \in \mathcal{V}$.*

The incidence graph is the same as the incidence poset after we forget the direction of the edges of the incidence poset. A related object is the line graph.

Definition 2 (Line graph). *The line graph of a graph $\mathcal{G} = (\mathcal{V}, \mathcal{E})$ is the graph $L(\mathcal{G})$ with vertices \mathcal{E} and an edge between $e, e' \in \mathcal{E}$ whenever e and e' share a common endpoint in \mathcal{G} .*

In the context of quantum Tanner codes, the following definition of Tanner code is usually taken, where the restriction of a vector $\mathbf{c} \in \mathbb{F}_2^{|\mathcal{E}|}$ defined on the edges \mathcal{E} of a graph to the local view of a vertex v is denoted \mathbf{c}_v . An ordering is assumed on the set of edges \mathcal{E} so that we may use $\mathbb{F}_2^{|\mathcal{E}|}$ instead of $\{\mathcal{E} \rightarrow \mathbb{F}_2\}$ as our vector space (in which case \mathbf{c}_v would be the composition $\mathcal{E}(v) \subseteq \mathcal{E} \xrightarrow{\mathbf{c}} \mathbb{F}_2$).

Definition 3 (Tanner code). *Let \mathcal{C} be a linear code of length Δ and $\mathcal{G} = (\mathcal{V}, \mathcal{E})$ be a Δ -regular graph, possibly with parallel edges but without self-loops. We define the Tanner code on \mathcal{G} and \mathcal{C} as*

$$\text{Tan}(\mathcal{G}, \mathcal{C}) \triangleq \{\mathbf{c} \in \mathbb{F}_2^{|\mathcal{E}|} : \mathbf{c}_v \in \mathcal{C} \text{ for all } v \in \mathcal{V}\}.$$

The definition assumes that \mathcal{G} has labeled local views. One may think of this as an order on each local view, where each order is (possibly) independent of the other orderings. Other definitions also exist, such as Tanner's original one [9]. It is often demanded that the graph \mathcal{G} is bipartite, so that one can put bits on one half of the vertices and constraints on the other half. This is essentially the same as allowing hypergraphs in Definition 3, and in particular, one has

$$\text{Tan}(\mathcal{G}, \mathcal{C}) = \text{Tan}'(I(\mathcal{G}), \mathcal{C}) = \text{Tan}(L(I(\mathcal{G})), \mathcal{C}),$$

where Tan' denotes the alternative definition of a Tanner code and $L(\mathcal{G})$ is the line graph of a graph \mathcal{G} .

Given a parity-check matrix \mathbf{H} , the *Tanner graph* of \mathbf{H} is the bipartite graph with one check node for each row of \mathbf{H} , one variable node for each column of \mathbf{H} , and an edge between variable node j and check node i whenever $H_{ij} = 1$. When rows of \mathbf{H} are combined into generalized checks through a collection $\mathcal{H} = \{\mathbf{H}_c\}_{c \in \mathcal{V}_c}$, for some set \mathcal{V}_c , such that

$$\mathbf{H} = \begin{bmatrix} \mathbf{H}_{c_1} \\ \vdots \\ \mathbf{H}_{c_{|\mathcal{V}_c|}} \end{bmatrix},$$

then the check nodes are \mathcal{V}_c . The variable nodes are the same as before, and we have an edge between c and v whenever column v of \mathbf{H}_c is nonzero. In other words, the Tanner graph for combined checks is the quotient graph of the original Tanner graph induced by the partitioning \mathcal{H} defines on the check nodes.

Our interest in studying (binary) parity-check matrices stems from their usefulness in describing quantum error correcting codes, particularly a type of code named after Calderbank, Shor, and Steane (CSS).

B. Quantum Error-Correcting Codes

Definition 4 (CSS code). *We say two classical linear codes $\mathcal{C}_0, \mathcal{C}_1$ form a CSS code $\text{CSS}(\mathcal{C}_0, \mathcal{C}_1)$ if they satisfy $\mathcal{C}_0^\perp \subseteq \mathcal{C}_1$.*

When the classical codes $\mathcal{C}_0, \mathcal{C}_1$ are given by parity-check matrices H_0, H_1 , respectively, the condition $\mathcal{C}_0^\perp \subseteq \mathcal{C}_1$ is equivalent to $H_0 H_1^\top = 0$, and we sometimes write $\text{CSS}(H_0, H_1)$ for the CSS code $\text{CSS}(\mathcal{C}_0, \mathcal{C}_1)$. If \mathcal{C}_0 and \mathcal{C}_1 have codelength n and dimension k_0 and k_1 , respectively, then $\text{CSS}(\mathcal{C}_0, \mathcal{C}_1)$ has length n and dimension $k = k_0 + k_1 - n$. Its minimum distance is $d = \min(d_X, d_Z)$, where

$$d_X = \min_{c \in \mathcal{C}_0 \setminus \mathcal{C}_1^\perp} |c|, \quad d_Z = \min_{c \in \mathcal{C}_1 \setminus \mathcal{C}_0^\perp} |c|.$$

We will next give a definition for quadripartite quantum Tanner codes. There are more general code constructions that are also called quantum Tanner codes [17], [21] for which the results of Section III still hold. However, the explicit quantum Tanner codes we consider in Section VI (see Table I) all fall under the following definition.

Let \mathcal{A}, \mathcal{B} be subsets of a group \mathcal{G} satisfying $\mathcal{A}^{-1} = \mathcal{A}$, $\mathcal{B}^{-1} = \mathcal{B}$, and $|\mathcal{A}| = |\mathcal{B}| = \Delta$ for some $\Delta \in \mathbb{N}$. The quadripartite left-right Cayley complex on $\mathcal{A}, \mathcal{B} \subseteq \mathcal{G}$ is defined as follows. It has vertices $\mathcal{V} = \mathcal{G} \times \{ij : i, j \in \{0, 1\}\}$, edges $\mathcal{E} = \mathcal{E}_A \cup \mathcal{E}_B$, where

$$\begin{aligned} \mathcal{E}_A &= \{((g, i0), (ag, i1)) : g \in \mathcal{G}, a \in \mathcal{A}, i \in \{0, 1\}\} \\ \mathcal{E}_B &= \{((g, 0j), (gb, 1j)) : g \in \mathcal{G}, b \in \mathcal{B}, j \in \{0, 1\}\}, \end{aligned}$$

and squares

$$\{[(g, 00), (ag, 01), (gb, 10), (agb, 11)] : a \in \mathcal{A}, g \in \mathcal{G}, b \in \mathcal{B}\}.$$

We write $\mathcal{V}_{ij} = \mathcal{G} \times \{ij\}$, $\mathcal{V}_0 = \mathcal{V}_{00} \cup \mathcal{V}_{11}$, and $\mathcal{V}_1 = \mathcal{V}_{01} \cup \mathcal{V}_{10}$. Qubits are placed on the squares, making the length of the code $n = |\mathcal{V}| \Delta^2 / 4 = |\mathcal{G}| \Delta^2$. Restrictions will be placed on the vertices \mathcal{V}_0 for the first part \mathcal{C}_0 of our CSS code, and on the vertices \mathcal{V}_1 for \mathcal{C}_1 . To align with Definition 3, we define, for $i \in \{0, 1\}$, the graphs \mathcal{G}_i^\square with vertices \mathcal{V}_i and an edge for each square, connecting the two vertices of \mathcal{V}_i that it is incident to.

Definition 5 (Quadripartite quantum Tanner code). *Given subsets \mathcal{A}, \mathcal{B} of a group \mathcal{G} satisfying $\mathcal{A}^{-1} = \mathcal{A}$, $\mathcal{B}^{-1} = \mathcal{B}$, and classical codes $\mathcal{C}_A, \mathcal{C}_B$ of length $\Delta = |\mathcal{A}| = |\mathcal{B}|$ and dimensions $k_A + k_B = \Delta$, the quadripartite quantum Tanner code on this data is $\text{CSS}(\mathcal{C}_0, \mathcal{C}_1)$, where*

$$\begin{aligned} \mathcal{C}_0 &= \text{Tan}(\mathcal{G}_0^\square, (\mathcal{C}_A \otimes \mathcal{C}_B)^\perp) \\ \mathcal{C}_1 &= \text{Tan}(\mathcal{G}_1^\square, (\mathcal{C}_A^\perp \otimes \mathcal{C}_B^\perp)^\perp). \end{aligned}$$

As noted already, the length of the quadripartite quantum Tanner code is $n = |\mathcal{G}| \Delta^2$. By counting checks in \mathcal{C}_0 and \mathcal{C}_1 , we get the bound $k \geq |\mathcal{G}|(\Delta^2 - 4k_A k_B)$ on the dimension. Given parity-check matrices $H_A, H_B, H_A^\perp, H_B^\perp$ for the classical codes $\mathcal{C}_A, \mathcal{C}_B, \mathcal{C}_A^\perp, \mathcal{C}_B^\perp$, respectively, we can use $H_A^\perp \otimes H_B^\perp$ and $H_A \otimes H_B$ as parity-check matrices for $(\mathcal{C}_A \otimes \mathcal{C}_B)^\perp$ and $(\mathcal{C}_A^\perp \otimes \mathcal{C}_B^\perp)^\perp$, respectively. These can then be used to make parity-check matrices for \mathcal{C}_0 and \mathcal{C}_1 where the row weights are multiples of row weights in H_A and H_B or H_A^\perp and H_B^\perp .

HGP codes are becoming a well-studied family of qLDPC codes. They can readily be used to construct families of quantum LDPC codes with constant rate and $\Theta(\sqrt{n})$ minimum distance as the codelength n tends to infinity.

Definition 6 (HGP code). *Given two matrices $A \in \mathbb{F}_2^{m_a \times n_a}$ and $B \in \mathbb{F}_2^{m_b \times n_b}$, the HGP code $\text{HGP}(A, B)$ is defined as the CSS code with parity-check matrices*

$$H_0 \triangleq [A \otimes I_{n_b} \quad I_{m_a} \otimes B^\top], \quad H_1 \triangleq [I_{n_a} \otimes B \quad A^\top \otimes I_{m_b}].$$

LP codes are lifted versions of HGP codes and are the first qLDPC code construction proven to yield asymptotically good codes.

Definition 7 (LP code). *Let $\hat{A} \in \mathbb{F}_2^{l m_a \times l n_a}$ and $\hat{B} \in \mathbb{F}_2^{l m_b \times l n_b}$ be block matrices consisting of $l \times l$ blocks, where the blocks of \hat{A} commute with the blocks of \hat{B} . Then the LP code $\text{LP}(\hat{A}, \hat{B})$ is the CSS code with parity-check matrices*

$$H_0 \triangleq [\hat{A} \otimes I_{n_b} \quad I_{m_a} \otimes \hat{B}^\top], \quad H_1 \triangleq [I_{n_a} \otimes \hat{B} \quad \hat{A}^\top \otimes I_{m_b}],$$

where the transpose is also taken inside the blocks (i.e., is the usual transpose), and \otimes is done on block-level.

C. Depolarizing Noise

For our numerical results in Section VI, we consider the depolarizing channel, where, for each qubit, X, Y, and Z errors happen with equal probability $\epsilon/3$, and the identity I happens otherwise.

Given a CSS code $\text{CSS}(H_0, H_1)$, we will view it as a stabilizer code by turning the rows of H_0 into X-type Pauli strings and the rows of H_1 into Z-type Pauli strings. Specifically, we replace 1 with X and Z, respectively, and replace 0 with I. These Pauli strings generate a subgroup of the n -fold Pauli group, which naturally acts on the state space for n qubits, $(\mathbb{C}^2)^{\otimes n}$. The stabilizer code defined by the CSS code is the fixed points of this action by the subgroup.

We will write $\langle \cdot, \cdot \rangle$ for the function that checks whether operators commute or not. Specifically, if two Pauli strings $\mathbf{F}_1, \mathbf{F}_2$ commute, we have $\langle \mathbf{F}_1, \mathbf{F}_2 \rangle = 0$, and otherwise $\langle \mathbf{F}_1, \mathbf{F}_2 \rangle = 1$. Given a set of stabilizers $\{\mathbf{F}_i\}$ for a code and a Pauli error \mathbf{E} , we get the syndrome s given by $s_i = \langle \mathbf{F}_i, \mathbf{E} \rangle$. When doing error correction, we want to guess the error \mathbf{E} (or an equivalent error) based on s . If some of the stabilizers are grouped together, we will write s_c for the part of the syndrome that comes from the stabilizers in the set c .

III. CYCLE STRUCTURE OF QUANTUM TANNER CODES

Here, we give a description of the 4-cycles of the Tanner graph of a quantum Tanner code, with and without combined checks. The results also hold for more general quantum Tanner codes than those of Definition 5, in particular the different generalizations in [17], [21]. We provide a way to construct codes where this graph will have a larger girth when combining only a constant number of checks. For this, the following definition is useful.

Definition 8 (2-TNC). *We say that subsets \mathcal{A}, \mathcal{B} of a group \mathcal{G} satisfy the 2-step Total No-Conjugacy (2-TNC) condition if*

$$agb \neq a'gb'$$

for all $(a, b) \neq (a', b') \in \mathcal{A} \times \mathcal{B}$ and $g \in \mathcal{G}$.

The 2-TNC condition ensures that there are no parallel edges in \mathcal{G}_0^\square and \mathcal{G}_1^\square . Therefore, we will say that a generalized quantum Tanner code satisfies the 2-TNC condition if there are no parallel edges in its \mathcal{G}_0^\square and \mathcal{G}_1^\square . By recombining the checks that we put on the vertices of \mathcal{G}_i^\square in the Tanner graph of \mathcal{C}_i , we get a bipartite graph with one check node for each vertex of \mathcal{G}_i^\square and one variable node for each edge of \mathcal{G}_i^\square , connected by an edge whenever the variable node comes from an edge adjacent to that vertex. In other words, we have the following lemma.

Lemma 1. *The incidence graph $I(\mathcal{G}_i^\square)$ is equal to the Tanner graph of \mathcal{C}_i where, for each vertex in \mathcal{G}_i^\square , the $k_A k_B$ checks associated with that vertex are combined.*

When combining checks as in Lemma 1, a BP_4 decoder will do message-passing on the combined graph $\mathcal{G}_{\text{comb}}^\square = (\mathcal{V}_v \sqcup \mathcal{V}_c, \mathcal{E})$, which can be described in the following way. Given a square complex \mathcal{X} , e.g., a left-right Cayley complex, let the set of variable nodes \mathcal{V}_v be the set of squares in \mathcal{X} and the set of check nodes \mathcal{V}_c be the vertices of \mathcal{X} . For each variable node, connect it to the four check nodes incident to that square by an edge. Since the square complex \mathcal{X} in the construction of a quantum Tanner code has a bipartition on its underlying graph (i.e., its 1-skeleton), the check nodes are naturally split into two sets, where one is used for X-checks and the other for Z-checks.

Proposition 1. $\mathcal{G}_{\text{comb}}^\square$ contains exactly these 4-cycles:

- 1) The 4-cycles associated to the parallel edges of \mathcal{G}_0^\square and \mathcal{G}_1^\square , which for the codes of Definition 5 correspond to $a, a' \in \mathcal{A}, b, b' \in \mathcal{B}, g \in \mathcal{G}$ such that

$$agb = a'gb'.$$

- 2) The 4-cycles from parallel edges of \mathcal{X} .
- 3) The 4-cycles coming from squares of \mathcal{X} sharing edges.

Proof: The 4-cycles in $\mathcal{G}_{\text{comb}}^\square$ correspond to two squares q, p in the square complex \mathcal{X} sharing (at least) two vertices $v, w \in \mathcal{V}_0 \sqcup \mathcal{V}_1$. When $v, w \in \mathcal{V}_0$, this corresponds to a pair of parallel edges in \mathcal{G}_0^\square , and similarly for \mathcal{V}_1 and \mathcal{G}_1^\square , accounting for the cycles or Item 1. The only other option is to have one vertex from each set, say $v \in \mathcal{V}_0$ and $w \in \mathcal{V}_1$. This can happen in only two ways: either q and p share a common edge, or they do not. If they do not share a common edge, v and w have a pair of parallel edges between them, so the 4-cycle is of the type of Item 2. In the other case, they are incident to the same edge between v and w , and we are in Item 3. ■

It is worth noting that each parallel edge of \mathcal{G}_A and \mathcal{G}_B leads to Δ parallel edges in \mathcal{G}_0^\square and \mathcal{G}_1^\square , and to 2Δ (assuming Definition 5) parallel edges in \mathcal{X} , where these are all the parallel edges there are. For the quadripartite quantum Tanner codes of Definition 5, all parallel edges of \mathcal{G}_A and \mathcal{G}_B come from repeated elements of \mathcal{A} and \mathcal{B} , respectively.

Proposition 1 describes the 4-cycles in the Tanner graph where the checks coming from the same vertex of \mathcal{X} are combined, which our proposed decoder can use for BP decoding. When checks are not combined, the additional checks

introduced by the local code must also be considered. Recall that the codes $\mathcal{C}_A^\perp, \mathcal{C}_B^\perp$ play an equivalent role to that of $\mathcal{C}_A, \mathcal{C}_B$ in the construction of a quantum Tanner code, so the local codes cannot all be good LDPC codes with Tanner graphs of large girth.

Proposition 2. *In the Tanner graph of \mathcal{C}_i , where H_i^{loc} is used as a parity-check matrix for the local code, we find the following 4-cycles.*

- (i) The 4-cycles of H_i^{loc} appear $|\mathcal{V}_i|$ times.
- (ii) Each pair of parallel edges of \mathcal{G}_i^\square labeled (a_1, b_1) and (a_2, b_2) in the same local view lead to

$$\begin{aligned} & ((H_i^{\text{loc}})_{a_1 \Delta + b_1, :} \cdot (H_i^{\text{loc}})_{a_2 \Delta + b_2, :}) \\ & \cdot \left((H_i^{\text{loc}})_{a_1^{-1} \Delta + b_1^{-1}, :} \cdot (H_i^{\text{loc}})_{a_2^{-1} \Delta + b_2^{-1}, :} \right) \end{aligned}$$

4-cycles.

In the Tanner graph for CSS($\mathcal{C}_0, \mathcal{C}_1$), we find the following 4-cycles between the X- and Z-checks.

- (iii) Each 4-cycle in $\mathcal{G}_{\text{comb}}^\square$ of edges labeled $(a_1, b_1), (a_2, b_2)$ and $(a_1^{-1}, b_1^{-1}), (a_2^{-1}, b_2^{-1})$ at a check-node of \mathcal{C}_0 and \mathcal{C}_1 , respectively, lead to

$$\begin{aligned} & ((H_0^{\text{loc}})_{a_1 \Delta + b_1, :} \cdot (H_0^{\text{loc}})_{a_2 \Delta + b_2, :}) \\ & \cdot \left((H_1^{\text{loc}})_{a_1^{-1} \Delta + b_1^{-1}, :} \cdot (H_1^{\text{loc}})_{a_2^{-1} \Delta + b_2^{-1}, :} \right) \end{aligned}$$

4-cycles. Furthermore, if either $a_1 = a_2$ or $b_1 = b_2$, this is a 4-cycle of type 3 of Proposition 1; otherwise it is of type 2.

For ease of notation, we stick to the quadripartite construction in Definition 5 for the following proof.

Proof: Each variable node corresponds to a square q with four vertices, as depicted below for the quadripartite construction:

$$\begin{array}{ccc} (gb, 10) & \xrightarrow{a \quad a^{-1}} & (agb, 11) \\ \left. \begin{array}{c} b^{-1} \\ b \end{array} \right| & q & \left. \begin{array}{c} b^{-1} \\ b \end{array} \right| \\ (g, 00) & \xrightarrow{a \quad a^{-1}} & (ag, 01) \end{array}$$

A 4-cycle must include two variable nodes, say coming from squares q_1 and q_2 as above, with a, g, b indexed by 1 and 2. For the q_1 and q_2 to be part of a 4-cycle, they must share at least one vertex. Any 4-cycle will include two check nodes, possibly equal. For the single vertex case, each vertex of \mathcal{V}_i has the restriction of H_i^{loc} placed on its local view, duplicating each vertex of H_i^{loc} $|\mathcal{V}_i|$ times.

For the 4-cycles including two different check nodes $c_1 \in \mathcal{V}_{i_1}$ and $c_2 \in \mathcal{V}_{i_2}$, we either have $i_1 = i_2$ or $i_1 \neq i_2$. In the first case, q_1 and q_2 both correspond to edges between c_1 and c_2 in $\mathcal{G}_{i_1}^\square$, that is, a pair of parallel edges in $\mathcal{G}_{i_1}^\square$. If $i_1 = i_2 = 0$, the columns of H_0 corresponding to q_1 will contain the columns $(H_0^{\text{loc}})_{a_1 \Delta + b_1, :}$ and $(H_0^{\text{loc}})_{a_1^{-1} \Delta + b_1^{-1}, :}$, and otherwise be zero. The column corresponding to q_2 similarly contains $(H_0^{\text{loc}})_{a_2 \Delta + b_2, :}$ and $(H_0^{\text{loc}})_{a_2^{-1} \Delta + b_2^{-1}, :}$, lining up in such a way that the inner product between the columns is precisely

$$((H_0^{\text{loc}})_{a_1 \Delta + b_1, :} \cdot (H_0^{\text{loc}})_{a_2 \Delta + b_2, :})$$

$$+ \left((H_0^{\text{loc}})_{a_1^{-1}\Delta+b_1^{-1},:} \cdot (H_0^{\text{loc}})_{a_2^{-1}\Delta+b_2^{-1},:} \right).$$

The number of 4-cycles between these two columns of H_0 is the number of ways to choose two from this sum of inner products. Among these, the number of ways to choose one from the first part of the sum and one from the second part of the sum gives us the desired number of 4-cycles.

When the two vertices c_1, c_2 are not both part of \mathcal{V}_0 , the situation is the same (possibly swapping a and a^{-1} or b and b^{-1}), apart from the matrix H_1^{loc} applying instead of H_0^{loc} for vertices in \mathcal{V}_1 . ■

The following corollary is immediate from Proposition 1.

Corollary 1. *If \mathcal{G}_i^\square has no parallel edges (satisfies 2-TNC) and the parity-check matrix for the local code contains t 4-cycles, then the Tanner graph of \mathcal{C}_i contains $t|\mathcal{V}_i|$ 4-cycles.*

When combining sets of $k_A k_B$ checks the natural way, the Tanner graph for \mathcal{C}_i has no 4-cycles. For quadripartite quantum Tanner codes (Definition 5), the girth of the graph is 8.

In [21], a version of quantum Tanner codes was considered, where the product code in the definition for a Tanner code is swapped for a bipartite graph of girth t . Similarly to Corollary 1, these codes can be made so that the Tanner graph of \mathcal{C}_i when combining checks has girth $2t$.

We may reasonably expect to see some improvement in decoding performance by combining only some of the checks from each vertex. In total, there are $k_A k_B$ checks for each vertex, so for an even split, we could combine any number dividing $k_A k_B$. In particular, if H_A and H_B^\perp have some wanted property, then combining the k_B checks in $H_A \otimes H_B$ and $H_A^\perp \otimes H_B^\perp$ corresponding to the same rows of H_A and H_B^\perp , respectively, might be a good middle ground. In that case, the proposed decoder would locally decode on $H_A \otimes [1 \dots 1]$ and $[1 \dots 1] \otimes H_B$. One could potentially decode the dual code locally, as well. For ease of later reference, we sum up some of the more natural strategies for grouping checks in the following remark, where \mathcal{C}_{SPC} is the single parity-check code of length Δ , with parity-check matrix $[1 \dots 1]$.

Remark 1. *Some natural ways to group the checks of a quantum Tanner code are:*

- 1) *Combine the $k_A k_B$ checks coming from the same vertex of \mathcal{G}_0^\square and \mathcal{G}_1^\square (the full grouping).*
- 2) *Combine k_A or k_B checks to obtain Tanner graphs for $\mathcal{C}_A^\perp \otimes \mathcal{C}_{\text{SPC}}$ and $\mathcal{C}_{\text{SPC}} \otimes \mathcal{C}_B$ or $\mathcal{C}_A \otimes \mathcal{C}_{\text{SPC}}$ and $\mathcal{C}_{\text{SPC}} \otimes \mathcal{C}_B^\perp$, respectively, and use this for each local view of respectively \mathcal{G}_0^\square and \mathcal{G}_1^\square (the partial grouping).*
- 3) *Apply an algorithm on H_0^{loc} and H_1^{loc} for combining checks that tries to minimize the size of the link of the check nodes, and use this for each local view of \mathcal{G}_0^\square and \mathcal{G}_1^\square , respectively (an unstructured local grouping).*
- 4) *Apply an algorithm on H_0 and H_1 for combining checks that tries to minimize the size of the link of the check nodes (an unstructured grouping).*

We will see later that strategies 1) and 2) of Remark 1 perform well in practice, and that a fairly simple greedy algorithm (Algorithm 1) in some cases can be used to beat

strategy 2) using strategy 3), see Section VI and Fig. 3. We have not so far observed strategy 4) beating strategy 1).

IV. CYCLE STRUCTURE OF HGP AND LP CODES

We will describe (some of) the 4-cycles of the Tanner graphs of HGP and LP codes, and how the proposed decoder can get rid of some of them. However, as shown in Section VI, the performance gain may be limited. This is likely because the construction allows for codes with very few 4-cycles to begin with, even none at all; see, for example, the codes C1 and C2 of [12].

Recall that HGP codes have parity-check matrices

$$H_0 \triangleq [A \otimes I_{n_b} \quad I_{m_a} \otimes B^\top], \quad H_1 \triangleq [I_{n_a} \otimes B \quad A^\top \otimes I_{m_b}].$$

In H_0 , the 4-cycles of A and B show up n_b and m_a times, respectively, and in H_1 , they show up n_a and m_b times, respectively. Other than that, there are no more 4-cycles, as the inner product between columns of $A \otimes I_{n_b}$ and columns of $I_{m_a} \otimes B^\top$ is at most 1, and the same holds for the blocks of H_1 . This implies the following proposition.

Proposition 3. *Given matrices $A \in \mathbb{F}_2^{m_a \times n_a}$ and $B \in \mathbb{F}_2^{m_b \times n_b}$ with t_a and t_b 4-cycles, respectively, then the Tanner graphs of H_0 and H_1 for HGP(A, B) contain $t_a n_b + t_b m_a$ and $t_b n_a + t_a m_b$ 4-cycles, respectively.*

Combining the checks coming from A (B), the resulting Tanner graphs contain t_b (t_a) 4-cycles.

In a scenario where B has many 4-cycles, we can get rid of them by combining checks according to collections of n_b checks in H_0 and m_b checks in H_1 . Furthermore, if B is a matrix that locally has many 4-cycles, we can get rid of them using smaller combined checks. Similarly for A . This might allow some freedom in the construction: one matrix can be chosen among matrices with “nice” structure, and the other among matrices that “fit together well” with the first, without the same requirement on its structure. Of course, they should both preferably be LDPC and define codes with large minimum distances.

As LP codes are lifted versions of HGP codes in the same sense as quadripartite quantum Tanner codes are lifted versions of dual product codes, the above analysis can be combined with the discussion in Section III to give a description of 4-cycles in LP codes, and how our proposed decoder can deal with them. The utility of this depends on how useful the added freedom in the choice of A, B is, at the cost of more complex decoding. In this regard, one should note that the pair A, B probably needs to be robust in the sense of product expansion for the LP code to have a good minimum distance.

V. PROPOSED DECODER

In this section, we outline the proposed iterative BP decoder. The main idea is to combine simple checks into more powerful checks and then process these using a trellis-based MAP decoder as part of the check node processing of each decoding iteration on the Tanner graph of the qLDPC code. A similar approach for improved decoding of binary linear codes was proposed in [22].

Algorithm 1: Check node combining

Data: An $m \times n$ parity-check matrix H_i and maximum size of blocks r .

Result: A collection \mathcal{H} of blocks of rows from H_i where each block contains at most r elements, and a Tanner graph $\mathcal{G}_i^{(r)}$.

- 1 $\tilde{H} \leftarrow H_i$, $\mathcal{H} \leftarrow \emptyset$, and $a \leftarrow 0$
- 2 $\mathcal{B} \leftarrow \{r, \dots, r, r-1, \dots, r-1\}$ such that $\sum_{b \in \mathcal{B}} b = m$
- 3 $\tilde{m} \leftarrow m$
- 4 **for** $b \in \mathcal{B}$ **do**
- 5 Set a to a random number in $[\tilde{m}]$
- 6 Set g to row number a of \tilde{H}
- 7 Set $\hat{H} \leftarrow g$
- 8 Delete row a of \tilde{H} ,
- 9 **for** $l \in [b-1]$ **do**
- 10 Compute $\tilde{H}g^\top$ and find the index of the maximum value, arbitrarily breaking ties
- 11 Remove the row r of that index from \hat{H}
- 12 $\hat{H} \leftarrow \begin{bmatrix} \hat{H} \\ r \end{bmatrix}$
- 13 $g \leftarrow g \vee r$
- 14 **end**
- 15 Set \tilde{m} to the number of rows of \hat{H}
- 16 $\mathcal{H} \leftarrow \mathcal{H} \sqcup \hat{H}$
- 17 **end**
- 18 Construct the Tanner graph $\mathcal{G}_i^{(r)}$ from \mathcal{H} , see Section II-A.
- 19 **return** \mathcal{H} , $\mathcal{G}_i^{(r)}$

For some code families, such as quantum Tanner codes, HGP codes, and LP codes, there are inherent structures that give natural ways to combine checks for generalized decoding. See Remark 1 for a discussion of how this can be done for quantum Tanner codes. There might be less apparent structures in the Tanner graph that are worse for the decoder than the obvious ones, and some code families might not have an obvious way to combine checks, like GB codes, so we give a greedy algorithm in Algorithm 1 for combining checks according to strategy 4) of Remark 1.

Next, we describe MAP decoding of the generalized checks, and then give the pseudo-code of the proposed iterative BP decoder.

A. Trellis-Based MAP decoder

The proposed trellis-based MAP decoder is outlined in Algorithm 2. It follows the standard forward/backward recursions of the BCJR algorithm in the logarithm domain, but adapted for a nonzero syndrome vector, i.e., the code trellis is modified by adding a coset leader (from the code coset corresponding to the syndrome vector) to all labelled paths (or codewords) in the trellis. A (minimal) code trellis for a linear block code can for instance be build using partial syndromes as outlined in [23]. We note that the complexity can be reduced by adopting a dual code approach as detailed for classical codes in [24] when the generalized check codes have rates above $1/2$.

Algorithm 2: Soft-input soft-output (SISO)

Data: Local parity-check matrix H_c , the corresponding syndrome vector s_c , the corresponding (ordered) messages from neighboring variables nodes $(\Gamma_0, \dots, \Gamma_{n_c-1})$, and the corresponding coset leader $u_c = u_c(s_c)$.

Result: Set of outgoing (ordered) messages to neighboring variable nodes $(\Delta_0, \dots, \Delta_{n_c-1})$

- 1 Construct a trellis $\mathcal{T}_c = (\cup_{t=0}^{n_c} \mathcal{S}_t, \cup_{t=0}^{n_c-1} \mathcal{E}_t)$, where $e \in \mathcal{E}_{t-1}$, with label $\ell(e)$, connects a state (or vertex) $s_l(e) \in \mathcal{S}_{t-1}$ to a state $s_r(e) \in \mathcal{S}_t$, based on H_c .
- 2 **for** $t \in [1 : n_c]$ **do**
- 3 **for** $s \in \mathcal{S}_t$ **do**
- 4 $\alpha_t(s) \leftarrow \max_{e \in \mathcal{E}^{(t-1)} : s_r(e)=s}^* (\alpha_{t-1}(s_l(e)) + (\ell(e) + u_{c,t-1})\Gamma_{t-1})$
- 5 **end**
- 6 **end**
- 7 **for** $t \in [n_c : 1]$ **do**
- 8 **for** $s \in \mathcal{S}_t$ **do**
- 9 $\beta_{t-1}(s) \leftarrow \max_{e \in \mathcal{E}^{(t-1)} : s_l(e)=s}^* (\beta_t(s_r(e)) + (\ell(e) + u_{c,t-1})\Gamma_{t-1})$
- 10 **end**
- 11 **end**
- 12 **for** $t \in [1 : n_c]$ **do**
- 13 $\Delta_{t-1} \leftarrow \max_{e \in \mathcal{E}^{(t-1)} : \ell(e)+u_{c,t-1}=0}^* (\alpha_{t-1}(s_l(e)) + \beta_t(s_r(e))) - \max_{e \in \mathcal{E}^{(t-1)} : \ell(e)+u_{c,t-1}=1}^* (\alpha_{t-1}(s_l(e)) + \beta_t(s_r(e)))$
- 14 **end**
- 15 **return** $(\Delta_0, \dots, \Delta_{n_c-1})$

The complexity of Algorithm 2 is proportional to the number of edges in the underlying trellis. The maximum number of trellis states for each depth is $2^{\min(k_c, n_c - k_c)}$ which can be reached at depth $\min(k_c, n_c - k_c)$ [23], if the input H_c is an $(n_c - k_c) \times n_c$ full-rank matrix. Moreover, there are k_c depths with two outgoing edges from each state, and $n_c - k_c$ depths with a single outgoing edge from each state. In general, the total number of edges can be seen to be at most

$$\begin{cases} 2(2^{k_c+1} - 2) + 2^{k_c}(n_c - 2k_c) & \\ = 2^{k_c}(4 + n_c - 2k_c) - 4 & \text{if } k_c \leq n_c - k_c \\ 2(2^{n_c - k_c + 1} - 2) + 2 \cdot 2^{n_c - k_c}(n_c - 2(n_c - k_c)) & \\ = 2^{n_c - k_c + 1}(2 - n_c + 2k_c) - 4 & \text{otherwise.} \end{cases}$$

When the checks of a quantum Tanner code are fully combined based on the local code structure, $n_c = \Delta^2$ and $k_c = k_A k_B$, while a partial combination gives $n_c \leq \Delta^2$ and $k_c \leq k_A k_B$. Furthermore, if the checks coming from H_A in $H_A \otimes H_B$ are combined, then the different n_c will be the products of Δ by the row weights of H_B . In Table I, we tabulate the total number of edges from the formula above, averaged over the generalized checks, for the different codes studied in this work.

Algorithm 3: Generalized BP₄ with memory (GMBP₄)

Data: A syndrome \mathbf{s} , a PCM $\mathbf{H} = \begin{bmatrix} \mathbf{H}_0 \\ \mathbf{H}_1 \end{bmatrix}$ where $\mathbf{H}_{0ij} \in \{1, \mathbf{X}\}$ and $\mathbf{H}_{1ij} \in \{1, \mathbf{Z}\}$, graphs $\mathcal{G}_i^{(r)} = (\mathcal{V}_i^{(r)} = \mathcal{V}_{c,i}^{(r)} \sqcup \mathcal{V}_v, \mathcal{E}_i^{(r)})$, $i \in \{0, 1\}$, local (binary) PCMs $\mathcal{H} = \{\mathbf{H}_c\}_{c \in \mathcal{V}_c^{(r)}}$ with coset leaders $\mathbf{u}_c = \mathbf{u}_c(\mathbf{s}_c)$, $c \in \mathcal{V}_c^{(r)}$, a maximum number of iterations T_{\max} , initial LLRs $\{\Lambda_v^W \in \mathbb{R}\}_{v \in \mathcal{V}_v, W \in \{\mathbf{X}, \mathbf{Y}, \mathbf{Z}\}}$, and a *flag* $\in \{0, 1\}$.

Result: A Pauli string $\hat{\mathbf{E}}$ such that $\langle \hat{\mathbf{E}}, \mathbf{H}_{i,:} \rangle = s_i$ for all i (success), or a Pauli string $\hat{\mathbf{E}}$ such that $\langle \hat{\mathbf{E}}, \mathbf{H}_{i,:} \rangle \neq s_i$ for some i (failure).

1 Initialization: Construct the Tanner graph

$$\mathcal{G}^{(r)} = \left(\mathcal{V}^{(r)} = \mathcal{V}_c^{(r)} \sqcup \mathcal{V}_v, \mathcal{E}^{(r)} \right)$$

where $\mathcal{V}_c^{(r)} = \mathcal{V}_{c,0}^{(r)} \sqcup \mathcal{V}_{c,1}^{(r)}$ and $\mathcal{E}^{(r)} = \mathcal{E}_0^{(r)} \sqcup \mathcal{E}_1^{(r)}$

2 $\Gamma_{v \rightarrow c}^W \leftarrow \Lambda_v^W$, $v \in \mathcal{V}_v \cong [n]$, $c \in \mathcal{E}^{(r)}(v)$, $W \in \{\mathbf{X}, \mathbf{Y}, \mathbf{Z}\}$

3 **for** $t \in [T_{\max}]$ **do**

4 **for** $i \in \{0, 1\}$, $c \in \mathcal{V}_{c,i}^{(r)}$, $v \in \mathcal{E}^{(r)}(c)$ **do**

5 $\Gamma_{v \rightarrow c} \leftarrow \log(1 + e^{-\Gamma_{v \rightarrow c}^{W_i}}) + \min(\Gamma_{v \rightarrow c}^{\mathbf{Y}}, \Gamma_{v \rightarrow c}^{W_i}) - \log(1 + e^{-|\Gamma_{v \rightarrow c}^{\mathbf{Y}} - \Gamma_{v \rightarrow c}^{W_i}|})$

6 **end**

7 **for** $c \in \mathcal{V}_c^{(r)}$ **do**

8 $\{\Delta_{c \rightarrow v}\}_{v \in \mathcal{E}^{(r)}(c)} \leftarrow \text{SISO}(\mathbf{H}_c, \mathbf{s}_c, \{\Gamma_{v \rightarrow c}\}_{v \in \mathcal{E}^{(r)}(c)}, \mathbf{u}_c(\mathbf{s}_c))$

9 **end**

10 **for** $v \in \mathcal{V}_v, W \in \{\mathbf{X}, \mathbf{Y}, \mathbf{Z}\}$ **do**

11 $\Gamma_v^W \leftarrow \Lambda_v^W + \frac{1}{\alpha} \sum_{\substack{c \in \mathcal{E}^{(r)}(v) \\ \langle W, \mathbf{H}_{cv} \rangle = 1}} \Delta_{c \rightarrow v}$

12 **end**

13 (Hard decision:) Let $\hat{\mathbf{E}} \in \{1, \mathbf{X}, \mathbf{Y}, \mathbf{Z}\}^n$ be the vector where $\hat{E}_v = 1$ if $\Gamma_v^W > 0$ for all $W \in \{\mathbf{X}, \mathbf{Y}, \mathbf{Z}\}$ and $\hat{E}_v = \text{argmin}_{W \in \{\mathbf{X}, \mathbf{Y}, \mathbf{Z}\}} \Gamma_v^W$ otherwise.

14 **if** $\langle \hat{\mathbf{E}}, \mathbf{H}_{i,:} \rangle = s_i$ for all rows $\mathbf{H}_{i,:} \subseteq \mathbf{H}$ **then**

15 **return** $\hat{\mathbf{E}}$

16 **end**

17 **for** $v \in \mathcal{V}_v, c \in \mathcal{E}^{(r)}(v), W \in \{\mathbf{X}, \mathbf{Y}, \mathbf{Z}\}$ **do**

18 $\Gamma_{v \rightarrow c}^W \leftarrow \Gamma_v^W - \frac{1}{\alpha} \langle W, \mathbf{H}_{cv} \rangle \Delta_{c \rightarrow v}$

19 **end**

20 **end**

21 **if** *flag* **then**

22 **return** OSD-1($\mathbf{H}, \{\Gamma_v^W\}_{v \in \mathcal{E}^{(r)}, W \in \{\mathbf{X}, \mathbf{Y}, \mathbf{Z}\}}$)

23 **end**

24 **return** $\hat{\mathbf{E}}$ (failure)

B. Improved BP Decoding Using Generalized Checks

The pseudo-code of the proposed decoder is given in Algorithm 3. It is based on the BP₄ decoder with memory effects (MBP₄) [3, Alg. 1], and has a flag for OSD post-processing. The selection of the scaling parameter α is important to optimize the performance for either the relatively high or the low error rate region, with an $\alpha > 1.0$ typically giving

improved performance for lower error rates (in the so-called error floor region). Note that we keep the scaling parameter α in Algorithm 3, rather than removing it, as they do in [3, Alg. 1], where this is referred to as fixed inhibition. This is because we observe better performance that way for the codes we have simulated.

The proposed decoder has an inherent complexity/performance trade-off in the sense that the size of the generalized checks from either Algorithm 1 or from the local codes can be made smaller (as discussed in Section III) in order to reduce the complexity of running Algorithm 2, which may lead to poorer decoding performance. This trade-off will be explored in the numerical results. Moreover, in order to lower the complexity further, we can run a hybrid version where the standard MBP₄ decoder is run first without OSD post-processing, and if it does not converge, we run Algorithm 3 with or without OSD post-processing.

The asymptotic complexity of our proposed decoder for quantum Tanner codes, Algorithm 3, is the same as for the standard (M)BP₄ decoder, i.e., $O(n)$, when the size of the local codes and the maximum number of iterations T_{\max} is kept constant. Constant-size local codes are indeed realistic, as the quantum Tanner codes are asymptotically good qLDPC codes in this case, at least if the constant Δ is large enough [8]. Note that all the inner for-loops are parallelizable in Algorithm 3 (and also in Algorithm 2). However, the constant cost of the trellis-based MAP decoder of Algorithm 2 can be daunting if the local codes are large, see Section V-A and Table I (last column). The OSD-1 we use here is the standard one, see [12]. The complexity of OSD- ω is $O(n^3 + n2^\omega)$.

VI. NUMERICAL RESULTS

Next, we compare the logical error rate decoding performance of qLDPC codes on the depolarizing channel, under MBP₄ with and without OSD of order 1 post-processing as in [12]; with and without MAP decoding of generalized check nodes.¹ We select $\alpha = 1.6$ ($\alpha = 1.5$ for the BB code) for our simulations, unless specified otherwise, and present results for three lengths $n = 144, 432/416/377$, and $686/688$. Unless specified otherwise, we use a maximum of 6 BP iterations in the simulations. For generalized decoding, we use a hybrid version where we first run the conventional MBP₄ decoder and if it does not converge, we run Algorithm 3, both using a maximum of 6 iterations. When using OSD post-processing, this step is only run after the second step of generalized decoding. We also compare with the recently introduced Relay-BP decoding algorithm in [4, Alg. 1]. Here, we adapt Relay-BP to a quaternary version referred to as Relay-BP₄ and given as Algorithm 4 in Appendix A.

In Fig. 1, we compare the performance of Algorithm 3 (MBP₄+OSD-1), without (solid curves) and with (dashed curves) MAP decoding of local codes. We compare the performance of the [144, 12, 12] BB code from [13] (red curves)

¹The BP₄ decoding part of our simulations is based on the implementation at <https://github.com/kit-cel/Quantum-Neural-BP4-demo> with the memory and OSD part implemented in house, together with the MAP decoder of the generalized checks.

TABLE I
LIST OF SIMULATED CODES^a

| $[[n, k, d]]$ | Construction | Row weight average | Row weight range | Figure | Source | Average trellis complexity upper bound (r combined checks) |
|-------------------------|--------------|--------------------|------------------|--------|--------|---|
| [[144, 12, 12]] | BB | 6 | 6 | 1 | [13] | 12(1), 14503(8) |
| [[144, 12, 12]] | GB | 8 | 8 | 1 | [25] | 16(1), 608(4), 15356(8) |
| [[144, 12, 11]] | QT | 9 | 9 | 1 | [18] | 18(1), 22652(9) |
| [[377, 25, 5]] | HGP | 6.75 | 6–7 | 2 | [26] | 13.5(1), 14402(8) |
| [[416, 18, ≤ 22]] | LP | 8 | 8 | 2 | [26] | 16(1), 1870(5) |
| [[432, 16, ≤ 26]] | QT | 13.31 | 12–16 | 2, 3 | [20] | 26.6(1), 449(3), 659(4), 3448(6), 212988(12) |
| [[432, 20, ≤ 22]] | QT | 9 | 9 | 2 | [18] | 18(1), 20476(9) |
| [[686, 34, 13]] | QT | 13 | 12–16 | 4 | [17] | 26(1), 221180(12) |
| [[686, 28, 14]] | QT | 13 | 12–16 | 4 | [17] | 26(1), 221180(12) |
| [[688, 30, ≥ 19]] | GB | 16 | 16 | 4 | [17] | 32(1), 52243(8) |

^aHere, QT stands for quantum Tanner code. For $r = 1$, we show the bound for the complexity of decoding the on dual code locally, as this is less complex and equivalent to the box-plus combining rule (see Algorithm 4 in Algorithm 4). For the $[[432, 16, \leq 26]]$ code, we give the average trellis complexity of the best performing grouping for $r = 3$ and 4 in Fig. 3. Note that when r is larger there are fewer checks to process in each BP decoding iteration.

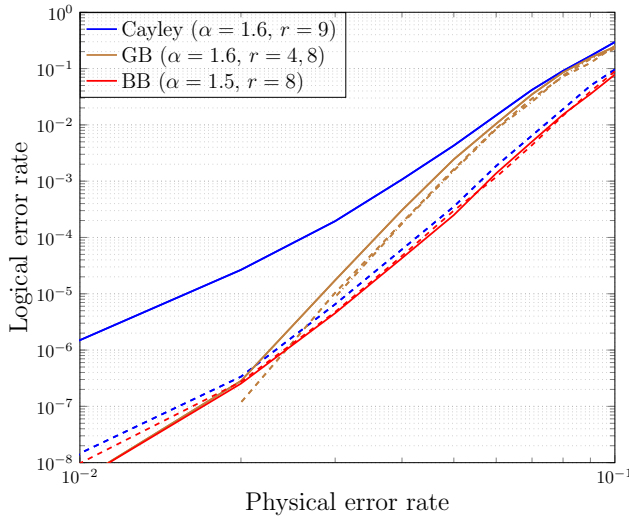


Fig. 1. Comparing the logical error rate performance of (generalized) MBP_4 +OSD-1 decoding (with $\alpha = 1.6$; $\alpha = 1.5$ for the BB code) of three different $[[144, 12]]$ qLDPC codes on the depolarizing channel. Solid curves are for standard MBP_4 +OSD-1 decoding, while dashed and dash-dotted curves are for generalized MBP_4 +OSD-1 decoding.

with that of an optimized $[[144, 12, 12]]$ GB code from [25] (brown curves) and the $[[144, 12, 11]]$ quantum Tanner code from [18] (blue curves). For the quantum Tanner code, we consider the full grouping (see Remark 1(1)), while Algorithm 1 is used to find a grouping for the GB and BB code (see also Remark 1(4)). From the figure, we can observe a significant performance improvement for the quantum Tanner code, while only modest gain for the GB and BB codes (the number of combined checks r is given in the legend). Interestingly, the quantum Tanner code performs comparably to the BB code under generalized (hybrid) decoding.

In Fig. 2, we show the corresponding results for length $n = 432/416/377$. We compare the performance of (generalized) MBP_4 decoding with and without OSD of order 1 post-processing (with $\alpha = 1.6$) of the $[[432, 20, \leq 22]]$ quantum Tanner code from [18] (dark blue curves), the $[[432, 16, \leq 26]]$ quantum Tanner code from [20, Tab. 2] (light blue curves), and the $[[416, 18, \leq 22]]$ LP code and the $[[377, 25, 5]]$ HGP code from the GitHub qLDPC code repository [26] (green and red curves). Solid curves are for standard MBP_4 +OSD-

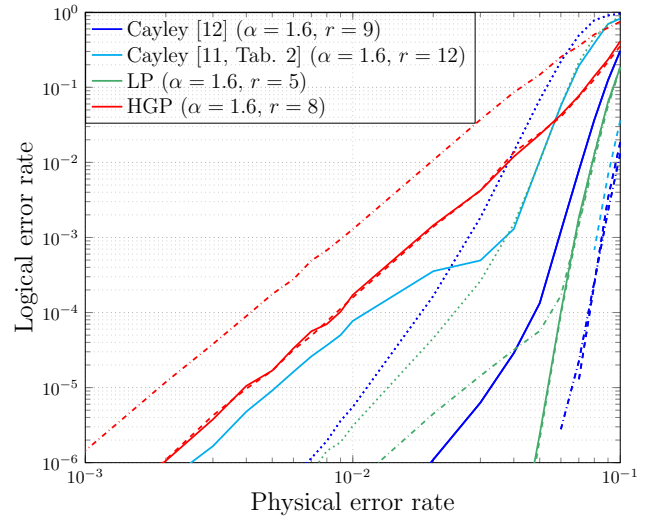


Fig. 2. Comparing the logical error rate performance of (generalized) MBP_4 decoding with and without OSD-1 post-processing (with $\alpha = 1.6$) of the $[[432, 20, \leq 22]]$ quantum Tanner code from [18] (dark blue curves), the $[[432, 16, \leq 26]]$ quantum Tanner code from [20, Tab. 2] (light blue curves), and the $[[416, 18, \leq 22]]$ LP code and the $[[377, 25, 5]]$ HGP code from the GitHub qLDPC code repository [26] (green and red curves) on the depolarizing channel. Solid curves are for standard MBP_4 +OSD-1 decoding, dashed curves are for generalized MBP_4 +OSD-1 decoding, while curves with dots are for decoding without OSD-1 post-processing (dotted curves for standard MBP_4 decoding with a maximum of 6 BP iterations and dash-dotted curves for generalized MBP_4 decoding with a maximum of 25 BP iterations).

1 decoding, dashed curves are for generalized MBP_4 +OSD-1 decoding, while curves with dots are for decoding without OSD of order 1 post-processing (dotted curves for standard MBP_4 decoding with a maximum of 6 BP iterations and dash-dotted curves for generalized MBP_4 decoding with a maximum of 25 BP iterations). The full grouping is used for the quantum Tanner codes (see Remark 1(1)), while Algorithm 1 is used globally for the LP code and locally for the HGP code. As for length $n = 144$, for both quantum Tanner codes, we can observe a significant performance improvement with generalized decoding, while for the LP and HGP codes there is no gain compared to conventional MBP_4 decoding. Moreover, it can be observed that OSD of order 1 post-processing boosts performance for both conventional and generalized MBP_4 decoding.

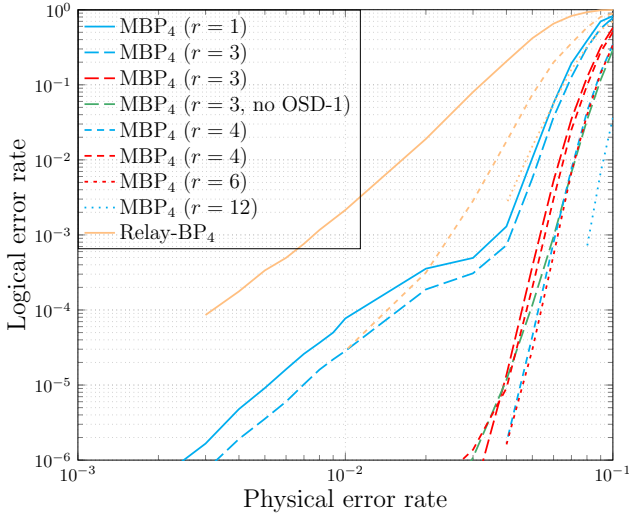


Fig. 3. Comparing the logical error rate performance of (generalized) $\text{MBP}_4+\text{OSD-1}$ decoding (with $\alpha = 1.6$) of the $[[432, 16, \leq 26]]$ quantum Tanner code from [20, Tab. 2] for different values of r on the depolarizing channel. The solid light blue curve is for standard $\text{MBP}_4+\text{OSD-1}$ decoding, and dashed to dotted light blue and red curves correspond (in this order) to increasing values of r ($r = 3, 4, 6, 12$). As a comparison, the performance of Relay-BP_4 (Algorithm 4) is shown with different values for the maximum number of relay legs (R in Algorithm 4) and the maximum number of BP iterations for each leg (T_r in Algorithm 4) (orange curves; the orange dotted curve has the same R and T_r as the dashed one, but with OSD-1 post-processing). The green curve is with no OSD-1 post-processing, but with a maximum of 50 BP iterations.

Next, in Fig. 3, we show the performance of (generalized) $\text{MBP}_4+\text{OSD-1}$ decoding (with $\alpha = 1.6$) of the $[[432, 16, \leq 26]]$ quantum Tanner code from Fig. 2, for different values of r to assess the performance-complexity trade-off of the proposed generalized MBP_4 decoder. The solid light blue curve is for standard $\text{MBP}_4+\text{OSD-1}$ decoding, and dashed to dotted light blue and red curves correspond (in this order) to increasing values of r ($r = 3, 4, 6, 12$). The light blue curves are for structured partial and full groupings, while the red curves are for unstructured local ones made with Algorithm 1, see Remark 1. Interestingly, there is a significant performance improvement even for unstructured $r = 3$ (while there is only limited improvement for the other $r = 3$). Increasing r to 4 improves the unstructured grouping only marginally, while the structured one is better. Increasing r to 6 does not bring any further gain over the best $r = 4$ curve, while increasing it all the way to 12 (structured full grouping) improves performance even further, but at the cost of a significant increase in decoding complexity (see Table I). This is likely because the 4×7 parity-check matrices used have more 4-cycles than the 3×7 ones, but in such a way that in the Kronecker product of these two, many of the 4-cycles are within blocks of three rows. This also shows that Algorithm 1 can be both better and worse than a structured grouping. As a comparison, the performance of Relay-BP_4 (Algorithm 4) with and without OSD of order 1 post-processing is shown as well (orange curves) with different values for the maximum number of relay legs (R in Algorithm 4) and the maximum number of BP iterations for each leg (T_r in Algorithm 4). The memory strengths for each leg are drawn independently and uniformly from a common range $[\gamma_c - \gamma_w/2, \gamma_c + \gamma_w/2]$ with

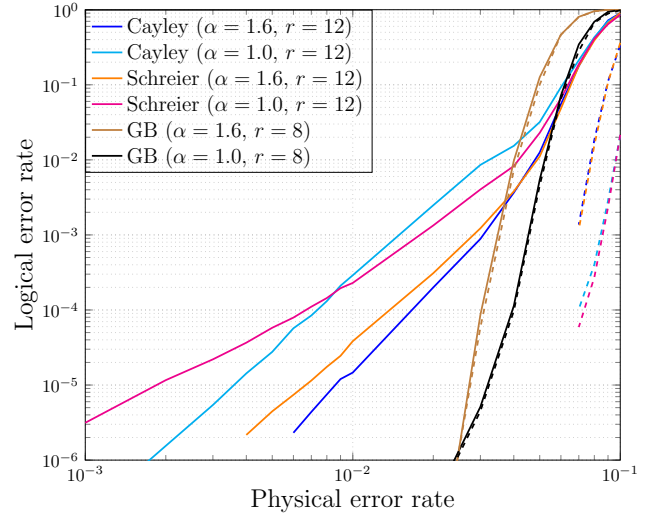


Fig. 4. Comparing the logical error rate performance of (generalized) $\text{MBP}_4+\text{OSD-1}$ decoding of two (generalized) quantum Tanner codes based on Cayley (dark and light blue curves) and Schreier (orange and magenta curves), respectively, and a GB code (brown and black curves) on the depolarizing channel for $n = 686$ (688 for the GB code). Solid curves are for standard $\text{MBP}_4+\text{OSD-1}$ decoding, while dashed curves are for generalized $\text{MBP}_4+\text{OSD-1}$ decoding. For all three codes, two different values for α (1.0 and 1.6) are compared.

$\gamma_c = 0.3$ (sweep optimized) and fixed $\gamma_w = 0.66$, and the number of solutions sought (S in Algorithm 4) is set equal to R . With modest values of $R = 5$ and $T_r = 6$, and no OSD post-processing, the performance (solid orange curve) is much worse than for $\text{MBP}_4+\text{OSD-1}$ decoding (light blue solid curve). Increasing R to 25 and T_r to 30 (which entails a significant increase in the overall number of BP iterations), yields a decent performance improvement (dashed orange curve), but it is still worse than the light blue solid curve. Adding OSD of order 1 post-processing on top, i.e., after each relay leg, does bring an additional benefit (dotted orange curve), but at a high computational cost. We also show a dashed green curve for $r = 3$ (with the same unstructured local groupings as for the red dashed curve), but with a maximum of 50 BP iterations and with no OSD-1 post-processing. Notably, this curve is better than the red dashed curve for error rates down to 10^{-5} where there is a crossing, i.e., removing the OSD post-processing and increasing the maximum number of BP iterations from 6 to 50 improves performance. Moreover, the performance is significantly better compared to the Relay-BP_4 curve with $R = 25$ and $T_r = 30$ (dashed orange curve), and with what appears to also be a lower decoding cost as the average trellis complexity of the generalized checks is 449 ($r = 3$; see Table I) which should be compared to $26.6 \cdot 3 \approx 80$ ($r = 1$, but with 3 times as many checks as for $r = 3$), while the maximum number of BP iterations is about 7.5 times higher for the Relay-BP_4 curve (orange dashed curve). Finally, we remark that adding OSD-1 post-processing on top of the green dashed curve (not shown) improves the performance only slightly, which is in contrast to standard MBP_4 decoding where typically it is difficult to come close to $\text{MBP}_4+\text{OSD-1}$ with a small number of BP iterations, by removing the OSD post-processing stage and increasing the number of BP iterations.

Finally, in Fig. 4, we show the corresponding results for length $n = 686/688$. Here, we compare the performance of an optimized $[[686, 28, 14]]$ generalized quantum Tanner code (from the Schreier construction; orange and magenta curves) with that of an optimized $[[686, 34, 13]]$ quantum Tanner code (from the Cayley construction; dark and light blue curves), both taken from [17, Tab. I]. For comparison, we also show the performance of an optimized $[[688, 30, \geq 19]]$ GB code [17, Tab. II] (brown and black curves). The performance with two different values of α is shown ($\alpha = 1.0$ and 1.6). As before, we use the full grouping for the quantum Tanner codes and Algorithm 1 to find an unstructured grouping for the GB code. Again, generalized decoding (dashed curves) gives enhanced performance (solid curves are for conventional decoding) for the two Tanner codes, while only a modest gain is observed for the GB code. Interestingly, here the Tanner codes outperform the GB code by a large margin. We also observe the effect of the two different values of α , with the smaller one showing improved performance for higher error rates. This is consistent with previous results from the literature.

VII. CONCLUSION AND FUTURE WORK

We proposed an improved iterative BP decoder for quantum Tanner codes that exploits the underlying local code structure by combining check nodes into more powerful generalized checks that are decoded using a MAP decoder as part of the check node processing of each decoding iteration. The proposed decoder significantly outperforms the standard quaternary BP decoder with memory effects, as well as the recently proposed Relay-BP decoder, at the expense of a higher decoding complexity, on the depolarizing channel. With the new decoder, we show that quantum Tanner codes can outperform GB and LP codes of comparable parameters, which shows that this class of codes can be competitive also in the finite codelength regime. Notably, combining checks into more powerful ones using a proposed greedy algorithm does not give noticeable gains for other classes of qLDPC codes, like LP and HGP codes. To explain the gain in performance for quantum Tanner codes, we showed how the 4-cycles of their Tanner graphs are reduced when combining checks, and gave a way to construct quantum Tanner codes where the Tanner graph has a designed girth when combining checks.

As future work, we will leverage the product structure of the local codes as well as investigate suboptimal SISO decoding algorithms for generalized checks to lower the decoder's overall complexity. It would also be interesting to see if good codes satisfying the 2-TNC condition can be constructed, and how they would perform under generalized decoding. Finally, evaluating the performance under circuit level noise models is an interesting avenue for further research.

APPENDIX A RELAY-BP₄

Below in Algorithm 4, we give the version of Relay-BP that we have run in our simulations, referred to as Relay-BP₄. Relay-BP₄ is a quaternary version of [4, Alg. 1]. In addition, we use the conventional box-plus check updating rule

in Algorithm 4 instead of the scaled-min check updating rule in [4, Eq. (1)].

REFERENCES

- [1] H. Yao, W. A. Laban, C. Häger, A. Graell i Amat, and H. D. Pfister, "Belief propagation decoding of quantum LDPC codes with guided decimation," in *Proc. IEEE Int. Symp. Inf. Theory (ISIT)*, Athens, Greece, Jul. 7–12, 2024, pp. 2478–2483.
- [2] S. Miao, A. Schnerring, H. Li, and L. Schmalen, "Quaternary neural belief propagation decoding of quantum LDPC codes with overcomplete check matrices," *IEEE Access*, vol. 13, pp. 25 637–25 649, 2025.
- [3] K.-Y. Kuo and C.-Y. Lai, "Exploiting degeneracy in belief propagation decoding of quantum codes," *npj Quantum Inf.*, vol. 8, no. 1, Sep. 2022, Art. no. 111.
- [4] T. Müller, T. Alexander, M. E. Beverland, M. Bühler, B. R. Johnson, T. Maurer, and D. Vandeth, "Improved belief propagation is sufficient for real-time decoding of quantum memory," Jun. 2025, arXiv:2506.01779v2 [quant-ph].
- [5] M. Ye, D. Wecker, and N. Delfosse, "Beam search decoder for quantum LDPC codes," Dec. 2025, arXiv:2512.07057v2 [quant-ph].
- [6] Z. Liu, A. Gong, and B. K. Clark, "Decoding quantum low density parity check codes with diffusion," Sep. 2025, arXiv:2509.22347v1 [quant-ph].
- [7] L. Valentini, D. Forlivesi, A. Talarico, and M. Chiani, "Restart belief: A general quantum LDPC decoder," Nov. 2025, arXiv:2511.13281v1 [quant-ph].
- [8] A. Leverrier and G. Zémor, "Quantum Tanner codes," in *Proc. 63rd Annu. IEEE Symp. Found. Comput. Sci. (FOCS)*, Denver, CO, USA, Oct. 31–Nov. 03, 2022, pp. 872–883.
- [9] R. M. Tanner, "A recursive approach to low complexity codes," *IEEE Trans. Inf. Theory*, vol. 27, no. 5, pp. 533–547, Sep. 1981.
- [10] D. Simegn, D. Artemasov, K. Andreev, P. Rybin, and A. Frolov, "Generalized LDPC codes with low-complexity decoding and fast convergence," *IEEE Wireless Commun. Lett.*, vol. 14, no. 11, pp. 3700–3704, 2025.
- [11] A. A. Kovalev and L. P. Pryadko, "Quantum Kronecker sum-product low-density parity-check codes with finite rate," *Phys. Rev. A*, vol. 88, no. 1, Jul. 2013, Art. no. 012311.
- [12] P. Panteleev and G. Kalachev, "Degenerate quantum LDPC codes with good finite length performance," *Quantum*, vol. 5, Nov. 2021, Art. no. 585.
- [13] S. Bravyi, A. W. Cross, J. M. Gambetta, D. Maslov, P. Rall, and T. J. Yoder, "High-threshold and low-overhead fault-tolerant quantum memory," *Nature*, vol. 627, no. 8005, pp. 778–782, Mar. 2024.
- [14] A. A. Kovalev and L. P. Pryadko, "Improved quantum hypergraph-product LDPC codes," in *Proc. IEEE Int. Symp. Inf. Theory (ISIT)*, Cambridge, MA, USA, Jul. 1–6, 2012, pp. 348–352.
- [15] J.-P. Tillich and G. Zémor, "Quantum LDPC codes with positive rate and minimum distance proportional to the square root of the blocklength," *IEEE Trans. Inf. Theory*, vol. 60, no. 2, pp. 1193–1202, Feb. 2014.
- [16] P. Panteleev and G. Kalachev, "Asymptotically good quantum and locally testable classical LDPC codes," in *Proc. 54th Annu. ACM Symp. Theory Comput. (STOC)*, Rome, Italy, Jun. 20–24, 2022, pp. 375–388.
- [17] O. Å. Mostad, E. Rosnes, and H.-Y. Lin, "Asymptotically good generalized quantum Tanner codes," *IEEE J. Sel. Areas Inf. Theory*, vol. 6, pp. 367–382, 2025.
- [18] A. Leverrier, W. Rozendaal, and G. Zémor, "Small quantum Tanner codes from left–right Cayley complexes," Dec. 2025, arXiv:2512.20532v1 [quant-ph].
- [19] R. K. Radebold, S. D. Bartlett, and A. C. Doherty, "Explicit instances of quantum Tanner codes," Aug. 2025, arXiv:2508.05095v3 [quant-ph].
- [20] L. Wang, A. Z. Liu, R. Li, A. Kubica, and S. Gu, "Check-weight-constrained quantum codes: Bounds and examples," Jan. 2026, arXiv:2601.15446v1 [quant-ph].
- [21] O. Å. Mostad, E. Rosnes, and H.-Y. Lin, "Improved construction of generalized quantum Tanner codes," in *Proc. Int. Symp. Topics Coding (ISTC)*, Los Angeles, CA, USA, Aug. 18–22, 2025.
- [22] E. Rosnes, "Iterative soft decoding of binary linear codes using a generalized Tanner graph," in *Proc. IEEE Inf. Theory Workshop (ITW)*, Paraty, Brazil, Oct. 2011, pp. 257–261.
- [23] J. K. Wolf, "Efficient maximum likelihood decoding of linear block codes using a trellis," *IEEE Trans. Inf. Theory*, vol. 24, no. 1, pp. 76–80, 1978.
- [24] G. Montorsi and S. Benedetto, "An additive version of the SISO algorithm for the dual code," in *Proc. IEEE Int. Symp. Inf. Theory (ISIT)*, Washington, DC, USA, Jun./Jul. 2001, p. 27.

- [25] O. Å. Mostad, H.-Y. Lin, E. Rosnes, D.-S. Lee, and C.-Y. Lai, “Advancing finite-length quantum error correction using generalized bicycle codes,” in *Proc. Int. Symp. Topics Coding (ISTC)*, Los Angeles, CA, USA, Aug. 2025, pp. 1–5.
- [26] A. Z. Liu, “Explicit QLDPC database,” Jan. 2026. [Online]. Available: <https://github.com/lilyxy/Check-weight-constrained-quantum-codes>

Algorithm 4: Relay-BP₄

Data: A syndrome s , a PCM $H = \begin{bmatrix} H_0 \\ H_1 \end{bmatrix}$ where $H_{0,ij} \in \{1, X\}$ and $H_{1,ij} \in \{1, Z\}$, initial LLRs $\{\Lambda_v^W \in \mathbb{R}\}_{v \in \mathcal{V}, W \in \{X, Y, Z\}}$, a number of solutions to be found S , a maximum number of legs for the relay R , a maximum number of iterations per leg T_r , and memory strengths for each leg $\{\gamma(r)\}_{r \in [R]}$.

Result: A Pauli string $\hat{\mathbf{E}}$ such that $\langle \hat{\mathbf{E}}, H_{i,:} \rangle = s_i$ for all i (success), or a Pauli string $\hat{\mathbf{E}}$ such that $\langle \hat{\mathbf{E}}, H_{i,:} \rangle \neq s_i$ for some i (failure).

```

1  $\hat{\mathbf{E}} \leftarrow \emptyset, s \leftarrow 0, \omega_{\hat{\mathbf{E}}} \leftarrow 0$ 
2  $\Gamma_v^W \leftarrow \Lambda_v^W, v \in \mathcal{V} \cong [n], W \in \{X, Y, Z\}$ 
3 for  $r \in [R]$  do
4   for  $v \in [n], W \in \{X, Y, Z\}$  do
5      $\Gamma_{v \rightarrow c}^W \leftarrow \Lambda_v^W$ 
6   end
7   for  $i \in \{0, 1\}, c \in \mathcal{V}_c, v \in \mathcal{E}(c)$  do
8      $\Gamma_{v \rightarrow c} \leftarrow \log(1 + e^{-\Gamma_{v \rightarrow c}^{W_i}}) +$ 
       $\min(\Gamma_{v \rightarrow c}^Y, \Gamma_{v \rightarrow c}^{W_i}) - \log(1 + e^{-|\Gamma_{v \rightarrow c}^Y - \Gamma_{v \rightarrow c}^{W_i}|})$ 
9   end
10  for  $t \in [T_r]$  do
11    for  $v \in [n], W \in \{X, Y, Z\}$  do
12       $\Lambda_v^W(t) \leftarrow (1 - \gamma_v(r))\Lambda_v^W + \gamma_v(r)\Gamma_v^W$ 
13    end
14    for  $c \in \mathcal{V}_c, v \in \mathcal{E}(c)$  do
15       $\Delta_{c \rightarrow v} \leftarrow (-1)^{s_c} \boxplus_{v' \in \mathcal{E}(c) \setminus \{v\}} \Gamma_{v' \rightarrow c}$ 
16    end
17    for  $v \in \mathcal{V}_v, W \in \{X, Y, Z\}$  do
18       $\Gamma_v^W \leftarrow \Lambda_v^W(t) + \sum_{\substack{c \in \mathcal{E}(v) \\ \langle W, H_{cv} \rangle = 1}} \Delta_{c \rightarrow v}$ 
19    end
20    for  $v \in \mathcal{V}_v, c \in \mathcal{E}(v), W \in \{X, Y, Z\}$  do
21       $\Gamma_{v \rightarrow c}^W \leftarrow \Gamma_v^W - \langle W, H_{cv} \rangle \Delta_{c \rightarrow v}$ 
22    end
23    for  $i \in \{0, 1\}, c \in \mathcal{V}_c, v \in \mathcal{E}(c)$  do
24       $\Gamma_{v \rightarrow c} \leftarrow$ 
       $\log(1 + e^{-\Gamma_{v \rightarrow c}^{W_i}}) + \min(\Gamma_{v \rightarrow c}^Y, \Gamma_{v \rightarrow c}^{W_i}) -$ 
       $\log(1 + e^{-|\Gamma_{v \rightarrow c}^Y - \Gamma_{v \rightarrow c}^{W_i}|})$ 
25    end
26    Let  $\hat{\mathbf{E}}(t) \in \{1, X, Y, Z\}^n$  be the vector where
       $\hat{E}_v(t) = 1$  if  $\Gamma_v^W > 0$  for all  $W \in \{X, Y, Z\}$ 
      and  $\hat{E}_v(t) = \operatorname{argmin}_{W \in \{X, Y, Z\}} \Gamma_v^W$  otherwise.
27    if  $\langle \hat{\mathbf{E}}(t), H_{i,:} \rangle = s_i$  for all rows  $H_{i,:} \subseteq H$  then
28       $\omega_r \leftarrow \omega(\hat{\mathbf{E}}(t)) = \sum_{v \in \mathcal{V}, \hat{\mathbf{E}}(t)_v = W \neq 1} \Lambda_v^W$ 
29      if  $\omega_r < \omega_{\hat{\mathbf{E}}}$  then
30         $\hat{\mathbf{E}} \leftarrow \hat{\mathbf{E}}(t)$ 
31         $\omega_{\hat{\mathbf{E}}} \leftarrow \omega_r$ 
32      end
33      break;
34    end
35  end
36  if  $s = S$  then
37    break;
38  end
39 end
40 return  $\hat{\mathbf{E}}$ 

```
